PERMAFROST AND PERIGLACIAL PROCESSES
*Permafrost and Periglac. Process.*, **22**: 378–389 (2011)
Published online in Wiley Online Library
(wileyonlinelibrary.com) DOI: 10.1002/ppp.737

# Advective Heat Transport in Frozen Rock Clefts: Conceptual Model, Laboratory Experiments and Numerical Simulation

Andreas Hasler,[1]* Stephan Gruber,[1] Marianne Font[2] and Anthony Dubois[2]

[1] Glaciology, Geomorphodynamics and Geochronology, Department of Geography, University of Zurich, Switzerland
[2] Laboratoire M2C, Université de Caen-Basse Normandie, UMR CNRS/INSU, Caen, France

## ABSTRACT

Advective heat transported by water percolating into discontinuities in frozen ground can rapidly increase temperatures at depth because it provides a thermal shortcut between the atmosphere and the subsurface. Here, we develop a conceptual model that incorporates the main heat-exchange processes in a rock cleft. Laboratory experiments and numerical simulations based on the model indicate that latent heat release due to initial ice aggradation can rapidly warm cold bedrock and precondition it for later thermal erosion of cleft ice by advected sensible heat. The timing and duration of water percolation both affect the ice-level change if initial aggradation and subsequent erosion are of the same order of magnitude. The surplus advected heat is absorbed by cleft ice loss and runoff from the cleft so that this energy is not directly detectable in ground temperature records. Our findings suggest that thawing-related rockfall is possible even in cold permafrost if meltwater production and flow characteristics change significantly. Advective warming could rapidly affect failure planes beneath large rock masses and failure events could therefore differ greatly from common magnitude reaction-time relations. Copyright © 2011 John Wiley & Sons, Ltd.

KEY WORDS: bedrock; permafrost; advective heat transport; conductive heat transfer; laboratory experiment; numerical modelling; rockfall; climate change

## INTRODUCTION

Mountain permafrost can be situated at high elevations above densely populated regions and in this steep topography it might condition debris flows or rockfalls, which in turn could trigger greater hazards downvalley. Climate change is expected to modify this hazard potential (Haeberli *et al*., 1997) and to affect the links between permafrost-related mass movements and atmospheric conditions (Haeberli and Beniston, 1998; Geertsema *et al*., 2006; Harris *et al*., 2001, 2009). Key questions are whether an increasing number of extremely hot summers will lead to more rockfalls in steep bedrock terrain, as in summer 2003 in the Alps (Gruber *et al*., 2004), and whether continued warming could cause large rock avalanches that differ markedly from historical events.

Both general thermal conditions and short-term thermal features must be comprehensively understood in order to investigate the temperature dependence of rock instability. In this context, it should be pointed out that: (1) the thermal conditions of recent rockfalls from permafrost areas are only known approximately and no correlation between these modelled rock temperatures and event frequency has been established (Noetzli *et al*., 2003; Fischer, 2010); and (2) much of the rockfall activity in the Alps in summer 2003 occurred earlier than the maximum active-layer thickness predicted from heat conduction (Gruber *et al*., 2004). Given the hypothesis that these rockfalls relate to thermal conditions at the failure planes, these two observations suggest that small-scale (cm to m) thermal anomalies caused by non-conductive effects may be significant.

Advective heat transport along clefts may be an important modifier of thermal and hydrological conditions and may influence the stability of ice-filled clefts in permafrost (Gruber and Haeberli, 2007). The quantification of this heat flux in steep, frozen bedrock is difficult because the physical processes are non-linear and natural conditions are heterogeneous and difficult to observe. For example, Hasler *et al*. (2011) measured significant thermal variability within the active layer of permafrost in steep bedrock, even on an annual basis, due to the cooling effects of thin snow cover and ventilation within clefts. Although short-term warming

* Correspondence to: A. Hasler, Department of Geography, University of Zurich, Winterthurerstr. 190, 8057 Zürich, Switzerland. E-mail: andreas.hasler@geo.uzh.ch

*Received 15 June 2010*
*Revised 2 November 2011*
*Accepted 2 November 2011*

effects were measured in some clefts, they had minor impacts on average thermal conditions. Investigations of the local heterogeneity of rock temperatures using geophysical methods have also led to thawing corridors being identified and these were attributed to advective heat input from percolating water (Krautblatter and Hauck, 2007).

In this paper, laboratory and numerical experiments are presented in relation to a conceptual hydrothermal model of a rock mass containing a single cleft. These reveal the sensitivity of linear thaw (ice erosion) along clefts and corresponding local permafrost degradation, and form a basis for future investigations of cleft assemblies in fractured rock. The following research questions are addressed: (1) Which processes are important for advective heat transport in rock clefts at sub-zero temperatures? (2) What are the effects of advection on cleft ice and temperatures around the cleft? (3) Which parameters govern the processes of advective heat transport?

The aim of the modelling is a semi-quantitative description of the thermal effects of advective heat transport in steep, fractured bedrock with permafrost, rather than a direct prediction of the small-scale thermal field in nature. The latter cannot be undertaken at present because the necessary information (detailed surface and near-surface characteristics) is not available. However, the general sensitivity of clefts in bedrock permafrost to advective heat input can be assessed and this provides a means to understand the impact of extreme climatic events and mean annual temperature rise on the thermal, hydrological and mechanical conditions of steep bedrock with permafrost.

## BASIS OF THE CONCEPTUAL MODEL

Hydrothermal processes in permafrost and seasonally frozen ground comprise the phase change of water and the transport of latent and sensible heat by the motion of water and water vapour. The importance of these processes varies with water content, hydraulic permeability and gradient, and depends on the scale considered. Hence, the near-surface characteristics and (micro-) topographic situation are significant factors.

### Hydrological Properties of Steep Bedrock containing Permafrost

High alpine mountain slopes have average inclinations between 40° and 70° and these rock masses contain discontinuities formed by orogenesis and weathering processes. Clefts defined as macroscopic discontinuities have typical apertures in the range of millimetres to decimetres and spacings of centimetres to metres from the near-surface to depths of decametres in this steeply sloping bedrock (e.g. Hasler *et al*., 2011). These structural properties shape the micro-topography and lead to great spatial heterogeneity in aspect and slope. The hydrological properties of this bedrock differ from permafrost in surficial deposits in gentle terrain (cf. Kane *et al*., 2001; Boike *et al*., 2008) because: (1) when unfrozen, water movement is dominated by flow along open clefts and moisture migration through the inter-cleft rock mass plays a minor role in low-porosity rock (Dietrich, 2005); (2) large hydraulic gradients (slope) and high permeability (macroscopic clefts) lead to mostly unsaturated conditions with preferential flow paths developed in the cleft system of the thawed near-surface layer; and (3) the cleft ice content controls hydraulic permeability in the permafrost body. In relation to the last point, it is often assumed that permafrost acts as an aquiclude in fractured bedrock or coarse-grained sediments providing the pore space is saturated (Rist, 2007). Observations of ice-filled clefts in the field (Gruber and Haeberli, 2007) indicate that this condition is often met in bedrock containing permafrost. Pumping experiments in fractured granite with and without permafrost also support this hypothesis (Pogrebiskiy and Chernyshev, 1977). Nevertheless, thermally eroded and progressively deepening channels within cleft ice cannot be excluded and deep-seated rock creep may render frozen fissures permeable by creating geometry changes.

Our model assumes an initially ice-sealed permafrost body with percolation along preferential flow paths and lateral runoff on the cleft ice surface (Figure 1). Rapid percolation in relatively wide clefts results in minimal heat exchange for water within the unsaturated zone, causing efficient heat transport to the cleft ice level (cf. Rist and Phillips, 2005, who observed similar effects in debris), which can be regarded as a heat transport shortcut between the surface (or atmosphere) and the ice level. The low depth of the water flow over the ice, however, may not be correct for very narrow clefts or clefts with sediment infill where heat exchange is expected to be less concentrated around the ice level. The temporal development of the ice level depends on the available water and thermal conditions. Water availability is limited during the cold season at high elevations, but in the spring, rock at several degrees below 0°C may be

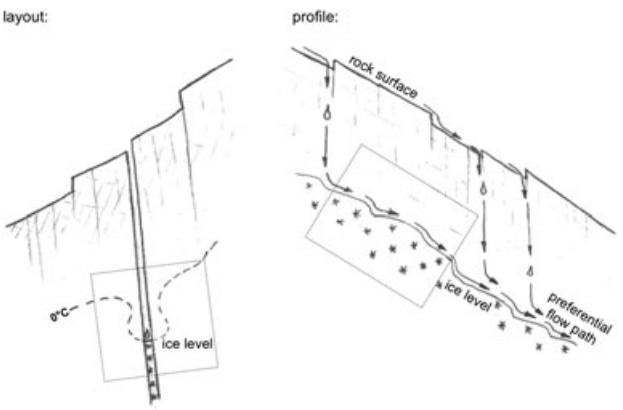


Figure 1 Sketch of hypothetical flow paths in the active layer or a talik within permafrost in bedrock. Left: cross-section through a rock cleft with the 0°C isotherm in summer (thawing front). Right: profile along a cleft with preferential percolation paths and runoff on the surface of the cleft ice. Dashed boxes: physical and numerical modelling domains.

subject to percolating meltwater (cf. Stähli *et al.*, 1996; Boike *et al.*, 1998; Scherler *et al.*, 2010). For this reason, ice aggradation is expected during the early thawing season before ice erosion becomes dominant.

### Heat Flow and Cleft Ice Evolution in a Rock Fracture

Advective heat transport to the subsurface comprises heat uptake in a source area at or near the surface, heat transport by water percolation and subsurface heat release. Heat uptake at the surface depends on various factors, causing a wide temperature range for the percolating water. Manual water temperature measurements at the rock surface at different sites and with differing weather conditions showed a range of 0.2–20°C for flow rates of 5 L $h^{-1}$ to several hundred litres per hour, which correspond to a sensible heat input of 20–10 000 W (Hasler, 2011).

Part of this heat is used to warm the surrounding rock while water percolates to the ice level. Water that arrives at the ice level with temperatures > 0°C may advect sensible heat ($P_{adv}$) because temperature at a macroscopic ice-water interface equilibrates at 0°C. This results in (1) warming by $\Delta T$ of the surrounding rock (and ice) mass with a corresponding change in liquid moisture content in the pores ($\Delta LWC$); and (2) geometry change (mass loss/gain) of the cleft ice as a function of the average cleft ice level ($\Delta z$) if the cleft aperture ($d_{cl}$) is constant (Figure 2). Accordingly, energy conservation in an advectively influenced cleft environment including conductive heat flux ($P_{cond}$) can be described as:

$$(P_{adv} + P_{cond}) \cdot t = \Delta T \cdot C_1 + \Delta z \cdot C_2 + \Delta LWC \cdot C_3 \qquad (1)$$

with the left-hand terms being heat input for a given duration ($t$) and the right-hand terms being the internal energy of the rock mass and latent heat change relating to cleft ice change and pore ice change. The constant $C_1$ is the heat capacity of the volume with changed temperature and $C_2$ and $C_3$ are the cleft geometry (width, length) and porewater content multiplied by the latent heat of fusion (Supplemental supporting material). $P_{adv}$ tends to zero when water that percolates into the cleft is at or close to 0°C, but heat transport still takes place when the latent heat of ice aggradation is released ($\Delta z > 0$) and absorbed by cold rock ($\Delta T$) around the cleft. If ice is eroded by $P_{adv}$, latent heat is consumed and exported from the system as runoff ($\Delta z < 0$). $\Delta LWC$ and $\Delta z$ are both reservoirs of latent heat but differ in their reversibility and feedbacks: liquid moisture that stays in place after melt will refreeze at the end of the thawing season and ground temperatures below the freezing transition indicate the enthalpy of the system and are interannually comparable. This is true for porewater because we consider average porewater content ($LWC$ + pore ice) to be constant due to the low hydraulic permeability of most rock types. Mass loss of cleft ice, which is much more mobile, reveals the enthalpy change and exports the advected energy with the eroded ice volume. Such geometry changes are important because the melt-interface will be at a new depth for subsequent events, modifying hydraulic and thermal conditions and changing the sensitivity to future thaw. These alterations in ground ice content can constitute a significant part of permafrost degradation but may be difficult to detect using ground temperature measurements.

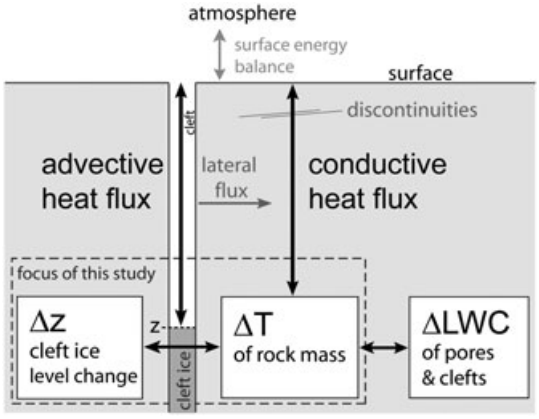


Figure 2 Conceptual model of heat flux components in bedrock with a cleft intersecting the surface and containing ice up to level $z$. Advective heat transport along the cleft and heat conduction in the rock mass result in changing rock temperature ($\Delta T$) and liquid water content ($\Delta LWC$) at depth and/or in a change of the ice level ($\Delta z$).

## METHODS AND SETUP OF MODELS

Our conceptual model of heat exchange was examined by focusing on a single cleft (Figures 1 and 2) using a combination of numerical analyses with a two-dimensional finite element model and physical experiments with an artificial cleft between two granite blocks in a cooling chamber.

The numerical model was formulated from the conceptual model with a heat conduction scheme and a moving ice-water interface. The fluid dynamics of the flow on this interface and the corresponding heat exchange with the ice and surrounding rock were parameterised with heat transfer coefficients. The laboratory experiment dimensions were chosen based on typical cleft dimensions (Hasler *et al.*, 2011) and initial numerical experiments to estimate the volume being thermally influenced by the cleft within the given time frame.

Experimental runs initially took place with constant heat input into the cleft (stationary experiments). These were used to calibrate the heat transfer coefficients to fit the observed ice-level changes. The numerical model was then used to investigate ice erosion and rock warming by systematically varying advective heat input, rock temperature and cleft size. In addition, combined forcing by transient surface temperature and advection (cyclic experiments) was applied to the laboratory experiments to simulate thawing after a

cold time period. Finally, scale effects and variable advective heat input were investigated numerically.

## Numerical Model

COMSOL Multiphysics software was used to solve the two-dimensional heat conduction equation and the moving boundary of the ice-water interface (Stefan problem). The model geometry corresponded to a cross-section perpendicular to a cleft and consisted of two rock sub-domains and simplified rectangular cross-sections of the water flow-body and ice within the cleft (Figure 3). The rock and ice sub-domains had an initialisation temperature $T_{rock}$ (initial condition). The driving variables of the model were either flow $Q$ and the mean water temperature ($T_w$) or the advective heat source ($P_{adv}$) and the upper and lower boundary conditions ($T_{up}$, $T_{bot}$). Heat flux through the lateral boundaries was set to zero corresponding to insulation in the laboratory experiments (Figure 3). To simplify the model, porewater was neglected ($\Delta LWC = 0$) and the rock was considered homogeneous and isotropic, corresponding to low-porosity rock and the laboratory settings (see below). To achieve a stable model operation and correct solution of the heat exchange at the moving boundaries (ice-water interface), the mesh was refined towards the cleft and model time steps were limited to 10 or 20 s. Both stationary and cyclic experiments are transient model runs and the term *stationary* refers only to the conditions of the driving variables (no steady-state modelling).

Flow characteristics (laminar or turbulent flow) along the ice surface in the cleft define the rate of heat exchange at the fluid-solid boundaries (water-ice and water-rock). Epstein and Cheung (1983) give a review of flow characteristics, heat exchange and interface instabilities at ice-water interfaces. Based on their model of simple phase change in an externally forced fluid flow, we used a heat transfer coefficient ($h_{int}$) as input to the phase change boundary. For initial modelling, standard values for $h_{int}$ for laminar flow of water over a flat surface were taken (2000 W m$^{-2}$ K$^{-1}$). However, positive feedbacks between the interface geometry and the flow are known to lead to turbulence and higher coefficients (Gilpin *et al*., 1980). Because the geometry of the rectangular flow cross-section in the model does not accurately represent real flow heights and geometry, the lateral heat transfer coefficient ($h_{side}$) is different from $h_{int}$. This difference is considered by a scaling factor ($sf$), which includes the effect of real flow height ($sf = h_{side}/h_{int}$).

The geometry change of the cleft ice was implemented via the moving mesh application mode of COMSOL. The melt-interface, that is the upper boundary of heat conduction in the ice sub-domain, was set at a constant 0°C and coupled to the water sub-domain via the heat transfer coefficient ($h_{int}$). The resulting heat flux discontinuity ($\Delta q_i = q_{i\_up} - q_{i\_down}$) was divided by the volumetric latent heat of fusion ($Lf$) and defined the velocity of the vertical displacement of the melt-interface $dz/dt$. The displacement of the interface was averaged over the cleft width ($d_{cl}$) to avoid lateral mesh deformation:

$$\frac{dz}{dt} = \frac{\Delta q_{i\_mean}}{Lf} = \int_{-d_{cl}/2}^{d_{cl}/2} \left(q_{i\_up} - q_{i\_down}\right) dx / (d_{cl} \cdot Lf) \quad (2)$$

Therefore the model reproduced the movement of the mean ice level but not the shape of the melt-interface. The water

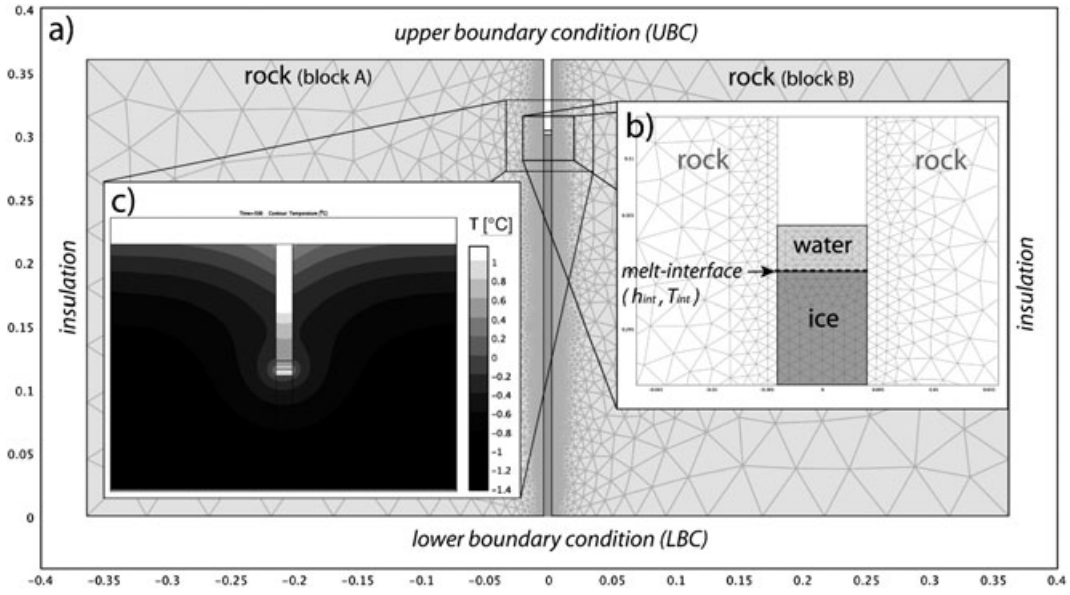


Figure 3 Geometry and mesh of the 8-mm cleft model and sample results: (a) overview of whole model; (b) close-up of ice-water interface within the cleft; (c) sample result at the end of a 500-s model run. The temperature at the melt-interface (ice-water) $T_{int}$ is defined as 0°C if a water flow is applied. The resulting heat flux discontinuity forces interface movement ($dz/dt$).

sub-domain was shifted according to the melt-interface velocity. The ice sub-domain was deformed by interface movement at the top and kept stable at the lower boundary.

The output of the model consisted of the temperature field, heat flux density and ice geometry for each time step. Heat fluxes through the boundaries of the water sub-domain and the velocity of the melt interface ($dz/dt$) were extracted as single values once they were in equilibrium (constant) or as a time slice if they were changing significantly. Model operation was verified by a visual check of the distributed model outputs, an evaluation of maxima and minima within the solutions, and cross-checking of the calculated heat fluxes and ice erosion rates.

## Laboratory Experiments

The laboratory experiments were conducted in a climate chamber in which temperature can be controlled between that of the outside air and approximately $-20$°C but is subject to fluctuations due to regulation and defrosting of the refrigerator. Strong ventilation prevents air stratification inside the cooling chamber and increases heat exchange at exposed surfaces. Additionally, a basal cooling plate controls the bottom temperature (Harris *et al.*, 2008).

The vertically dipping single cleft was formed between two inclined granite blocks with a spacing ($d_{cl}$) of approximately 4 and 8 mm. The blocks were insulated at their sides to minimise lateral heat flux through these boundaries. The cleft was filled with ice (water frozen *in situ*) up to a defined initial ice level (Figure 4). The ice level was kept parallel to the surface ($\alpha = 12°$) or at an inclination of $\alpha = 3°$ or $\alpha = 30°$ for the stationary experiments and at 12° as an initial condition of the cyclic experiments. A controlled discharge $Q$ at a temperature $T_w$ flowed along the cleft.

The temperature at the surface ($T_{up}$) was controlled by the cooling room, and the bottom was kept at a constant temperature ($T_{bot}$) by the basal cooling plate. Granite with low porosity ($< 0.5\%$) and homogeneous characteristics was used to minimise anisotropy and latent heat effects of porewater ($\Delta LWC$ close to 0). Sawed cleft surfaces had a reduced roughness and a more constant cleft width compared to natural situations. This allowed quantification of ice volume changes by simple ice-level measurements but may have led to more uniform flow conditions than in natural clefts. Water was cooled to the input temperature ($T_{win}$) by a looped copper tube in an ice-water bath and the flow rate was regulated by a mechanical valve. The stability of $Q$ and $T_{win}$ was low due to feedbacks between flow and water temperature and could not be easily controlled to the desired input temperature.

Experiments were defined by the input parameters specified for each run: initial model temperature ($T_{rock}$) and the driving variables $T_{win}$, $Q$, $T_{bot}$ and $T_{up}$. Result variables were the recorded ice-level changes ($\Delta z$) and temperatures within the model. The vertical distance of the ice level to the block surface was manually measured at five positions

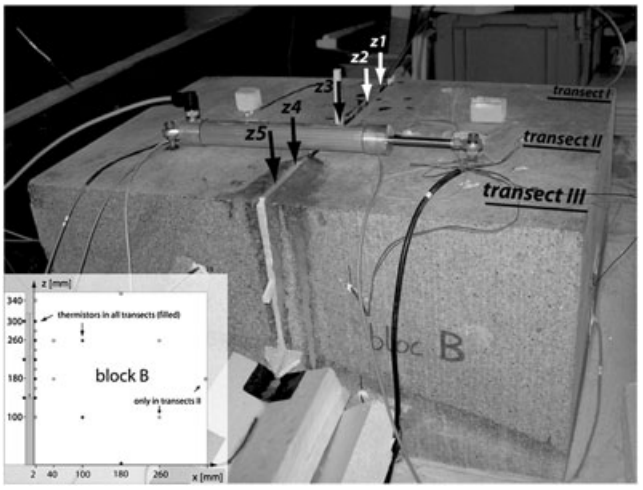


Figure 4 Setup of the laboratory experiment. Two granite blocks (0.36 x 0.36 x 0.5 m) form a cleft of approximately 8-mm (or 4-mm) width. The water flows from the rear to the front, where it is captured by a polystyrene spout and the water temperature is measured with a thermistor before it leaves the experiment (front). On top, a crack-meter is mounted across the cleft to record cleft aperture. Ice levels are measured at five positions along the cleft (z1 to z5). Inset figure: dots indicate where rock temperatures are measured within the three transects (I-III); thermistors are identified according to x-coordinate and z-coordinates (e.g. 2_340 is the uppermost thermistor near the cleft).

(50, 150, 250, 400 and 450 mm from the inlet side) using a ruler with a precision of $\pm$ 2 mm. These raw values were used to calculate the respective ice levels z1 to z5 and average ice-level change ($\Delta z$). The spatial distribution of rock temperatures was measured by a total of 50 thermistors placed in three transects (I = 50 mm, II = 250 mm and III = 450 mm from the inlet) perpendicular to the cleft at 2, 40, 100 and 260 mm from the cleft (Figure 4). These temperatures are labelled according to the distance from the cleft and the height (z-axis) (Figure 4). The boundary temperatures of block B were measured using thermistors at the rock surface and the sides and bottom of the block (Figure 4, right block). Cleft aperture ($d_{cl}$) was observed with a crack-meter at the top of the blocks and the output water temperature ($T_{wout}$) was measured in the funnel below the model (Figure 4).

A 60-channel Agilent 34970A (Agilent, Santa Clara, USA) data acquisition system was used together with thermistors (YSI-44031, YSI Inc., Yellow Springs, USA) having an absolute accuracy of $\pm 0.05$°C around the calibration point of 0° C. The thermistors were calibrated before instrumentation in a double-walled ice-water bath. The measurement accuracy of the water temperatures $T_{win}$ and $T_{wout}$ was $\pm 0.2$° C due to the influence of ambient temperature at the lowest flow rates and better if $Q > 10$ L h$^{-1}$. Water flow was measured using multi-purpose Digmesa FHKSC (Digmesa AG, Stansstad, Switzerland) flowmeters which have an absolute accuracy of $\pm$20 per cent, but better relative accuracy for temporal variations. Values were recorded every 10 s for stationary experiments and every minute for cyclic experiments.

### Calculation of Heat Input ($P_{adv}$) and Latent Heat Flux ($P_{lat}$)

Two main heat fluxes needed to be defined to link the laboratory experiments to the numerical modelling. $P_{adv}$ is calculated by the cooling of water within the cleft $(T_{win} - T_{wout})$ multiplied by $Q$ and the heat capacity of water ($C_w$) in J m$^{-3}$ K:

$$P_{adv} = Q \cdot (T_{win} - T_{wout}) \cdot C_w \quad (3)$$

If Q is in L h$^{-1}$, a denominator of 3.6 x 10$^6$ must be added to Equation 3 to obtain W. For varying fluxes and temperature differences such as the case in some laboratory experiments, $P_{adv}$ needed to be calculated for each point in time and subsequently averaged.

$P_{lat}$ is deduced from the erosion rate ($dz/dt$) multiplied by the cleft width ($d_{cl}$), the length of the cleft ($l$) and the latent heat of fusion ($Lf$):

$$P_{lat} = Lf \cdot 0.917 \cdot d_{cl} \cdot l \cdot \frac{dz}{dt} \quad (4)$$

For the non-standard units used here, Equation 4 needs to be multiplied by 6 x 10$^{-5}$ to obtain W. The factor of 0.917 is due to the lower density of ice compared to water. For the two-dimensional modelling, these heat fluxes values are divided by the length ($l$) of the experiment.

### Model Runs and Calibration

Rock and water temperatures and heat input during the stationary laboratory experiments covered the following ranges: $T_{win}$ varied between 0° and 6° C, $Q$ was in the order of 4 to 60 L h$^{-1}$ and $T_{rock}$ was in the range of −1° to −6°C. Variation was not completely systematic due to limitations in the control of $Q$ and $T_{win}$. These ranges do not span all possible values in nature in the near-surface but are reasonable for conditions at depths of up to a few metres in alpine permafrost. Detailed information on the settings used in the laboratory experiments is provided in the Supplemental supporting material (Supplemental Table 1). The numerical simulations of the stationary experiments reproduced these settings for model calibration before cyclic variation was applied.

The surface temperatures in the cyclic experiments fluctuated between −4° and +4°C and water flow ($Q$) of a total volume ($V_w$) was applied after a time delay ($\Delta t$). $Q$ was limited to approximately 5 L h$^{-1}$ so the duration of the advection event depended mainly on the applied water volume ($V_w$). The water temperature was kept as constant as possible around 2°C for all experiments and only $V_w$ and $\Delta t$ varied. A detailed list and graphs of the cyclic experiment settings are included in the Supplemental supporting material.

The heat transfer coefficient ($h_{int}$) and scaling factor ($sf$) of the numerical model depend on the flow conditions, which result from the flow rate, the cleft width and the inclination of the ice surface. Assuming Reynolds numbers in the order of $10^2$ to $10^3$ derived from average flow velocity observations in the laboratory, we expected laminar flow in the open channel. However, step formation observed at the melt-interface and retrograde erosion at the model outlet indicated local turbulence. To estimate the scaling factor, we neglected these features and used a simple approximation of the flow height based on the flow velocity measurements. A linear function was used to parameterise this scaling factor as dependent on Q and $d_{cl}$ (Supplemental supporting material). The value of the scaling factor has a minor influence on the model results.

The heat transfer coefficient ($h_{int}$) was determined by two different calibration procedures (Supplemental supporting material). Both methods provide parameters in the same order of magnitude. A linear function for the flow-dependent heat transfer coefficient was used for each cleft size (Supplemental supporting material). If $T_w$ is used as a driving variable, errors of $h_{int}$ propagate proportionally to the resulting erosion rate and warming of ice. For model runs driven by $P_{adv,}$ the influence of $h_{int}$ is only significant when erosion rates are close to zero. $P_{adv}$ was used as a driving variable for all experiments except for the analysis of scale effects.

## RESULTS

### Laboratory Experiments

Several qualitative and semi-quantitative observations were made during the experiments that are important for interpretation of the quantitative results. One to four steps, 2–5 cm high, formed in the cleft ice surface with the exception of when the ice was inclined at only 3°. These irregularities affected those stationary experiments with strong erosion as well as the cyclic experiments. Frontal erosion of the ice occurred at the lower side of the cleft (water outlet, close to *z5*) and an over-deepening of the ice-water interface developed at the water inlet (at *z1*). This required sealing the upper end of the cleft to avoid water loss. Some ice remained on the lateral cleft surfaces at low rock temperatures so the entire cleft ice volume within $dz$ was not subject to melt. These observations indicate the importance of flow conditions for local ice erosion rates and the potential for warm water to cause rapid ice erosion. For each stationary experiment, water temperatures within the cleft were measured intermittently, indicating a linear temperature decrease along the cleft. The cleft width ($d_{cl}$) did not change significantly as long as the model remained frozen.

The results of one stationary experiment are shown in Figure 5a. The advective heat flux according to Equation 3 and the erosion rate in the middle (z3) of the experiment were constant (black line). The higher erosion rate at z5 resulted from frontal erosion at the experiment outlet. The near-cleft temperatures (at z = 300 and 280 mm) increased until the ice level and corresponding water flow reached the level of the thermistor. Subsequently, the temperature dropped again with a slightly lower gradient. When two thermistors were passed

by the erosion surface, the time between two temperature peaks indicated the erosion rate at this transect (Figure 5a). For the experiment shown, this value corresponded well with the manual measurements of ice erosion.

The average ice erosion rate based on all ice-level measurements was calculated for the stationary experiments. These rates depend on cleft width, advective heat input and initial rock temperature (Figure 5b). The number of experiments is not sufficient to quantify these relations empirically, but Figure 5b indicates that the erosion rate correlates with the applied advective heat for similar cleft widths and initial rock temperature ($T_{rock}$). The lines in Figure 5b indicate the maximum erosion calculated by Equation 4 assuming that all heat is transformed into ice melt ($P_{lat}/P_{adv} = 1$). Erosion rates exceeded this theoretical limit in one experiment (Figure 5b, stat_13, red square at 47 W). The water temperature had a further influence on the erosion rate because higher water temperatures at the same $P_{adv}$ (larger $T_{win}$ and smaller flow Q) result in more ice erosion ($P_{lat}/P_{adv}$ is larger). However, this effect was minor compared to the influence of $P_{adv}$ and $T_{rock}$. The inclination ($\alpha$) also had an influence on flow conditions ($h_{int}$ in the model) and modified heat input ($P_{adv}$) (Supplemental supporting material). This explains the observed frontal erosion and may control the along-cleft form of the ice level.

The input parameters and other variables of interest in one cyclic experiment are shown in Figure 6a. The near-cleft temperatures at the ice level showed an abrupt increase when water was applied. A significant modification of conductive warming was also observed at the thermistors at 40-mm distance to the cleft. The applied advective heat per cycle is proportional to the water volume ($V_w$) (light blue area) if the water temperature remains constant, as was intended for all experiments. This was not the case, however, and $T_{win}$ was significantly different from 2°C for some cycles (Figure 6a). Consequently, $V_w$ and $\Delta t$ were used as common settings that define cycle classes and the variability in $T_{win}$ affected the spreads (boxplot) in ice erosion per cycle within these classes (Figure 6b; Supplemental supporting material). Step formation in the ice surface accumulating over several cycles may have been a further reason for the large spreads. Nevertheless, a qualitative dependency of ice erosion on $V_w$ and $\Delta t$ is apparent, with timing of the applied advective heat and the amount of heat of comparable importance (Figure 6b).

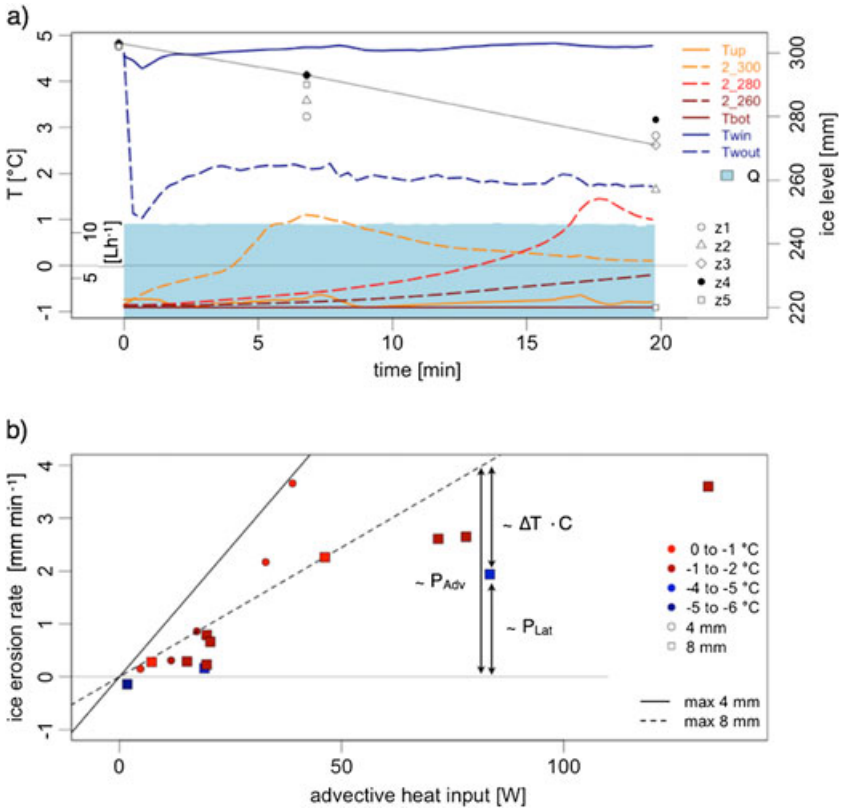


Figure 5 Results from the stationary laboratory experiments: (a) measured driving variables ($T_{up}$, $T_{bot}$, $T_{win}$, $Q$), rock temperatures of transect II near the cleft (2_300, 2_280, 2_260) and ice levels ($z1$-$z5$) for experiment stat_5 (4-mm cleft, Q = 12 L h$^{-1}$, $T_{win}$ = 4.7°C). The line for $z3$ indicates an erosion rate of 1.6 mm min$^{-1}$. The time difference between the two peaks indicates 20 mm of erosion in 11 min (1.8 mm min$^{-1}$); (b) ice erosion rates for different cleft sizes (point shape) as a function of applied advective heat flux ($P_{adv}$): point colours indicate rock temperature at the start of the experiment; the lines correspond to the maximum erosion rates when all applied energy is used for ice melt only; $P_{lat}$ of one experiment is proportional to the distance from 0 mm min$^{-1}$ erosion and the distance to the corresponding line is proportional to advective warming of the rock (examples shown by arrows). Symbols are given in the List of Terms.

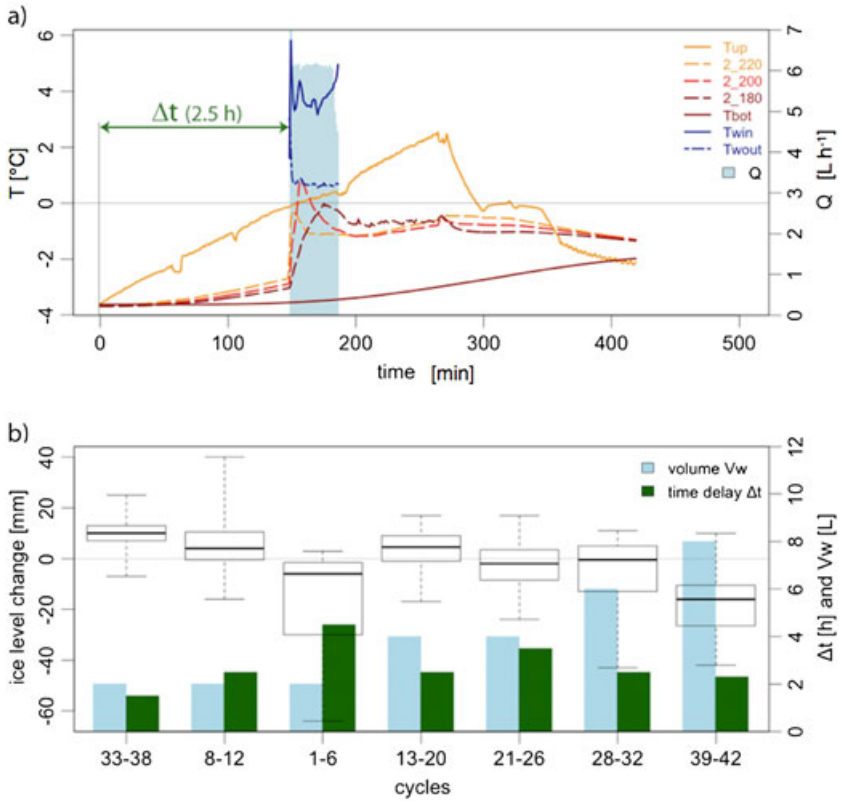


Figure 6 Results from the cyclic laboratory experiments: (a) boundary conditions, flow $Q$, water temperatures ($T_{win}$, $T_{win}$), and near-cleft rock temperatures for the warm period of cycle 30; (b) ice erosion per cycle, ordered by applied water volume ($V_w$) and time delay ($\Delta t$). The boxplot indicates the spread (variance (box) and extreme values (whiskers)) of all ice-level changes (z1 to z5) of the different cycles with similar settings. Symbols are given in the List of Terms.

## Numerical Model

Figure 7 shows the near-cleft rock temperatures for a model run with $P_{adv}$ and $T_{rock}$ settings similar to those of the laboratory experiment stat_5. The amplitudes and time lags for two modelled temperatures (m_300 and m_280) correspond well with those for the thermistors 2_300 and 2_280 in the experiment. It should be noted that these temperatures were not used for the calibration of $h_{int}$ (Supplemental supporting material) so this accord indicates that the model is operating correctly. In experiment stat_5, the ratio $P_{lat}/P_{avd}$ was 20 W/33 W, while the modelled ratio for the corresponding settings is 19.2 W/33.3 W.

The evolution of the modelled ice level ($\Delta z$) for different $P_{adv}$ and $T_{rock} = -3°C$ is shown in Figure 8. For large heat input ($P_{adv} > 20$ W), ice erosion starts within seconds after model initialisation. If $P_{adv}$ is low, however, significant ice aggradation occurs. Similar aggradation was observed in the laboratory experiments (Figure 5b, negative erosion rate). The aggradation was greatest at the start of the advective heat flux due to the large sensible heat flux towards the sub-zero cleft environment. For simulations with moderate heat input

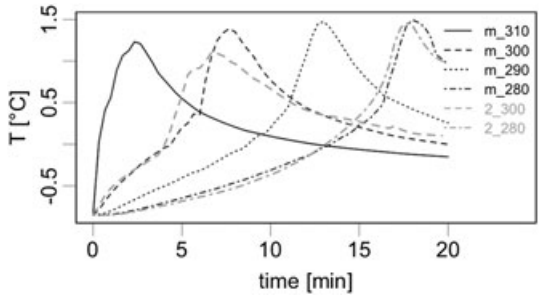


Figure 7 Numerical model results (m_310 ... m_280) and measured (transect II 2_300, 2_280) near-cleft rock temperatures (2 mm from cleft surface) in a 4-mm wide cleft. The settings correspond to experiment stat_5 ($T_{rock} = -0.85°C$, $P_{adv} = 33$ W). Symbols are given in the List of Terms.

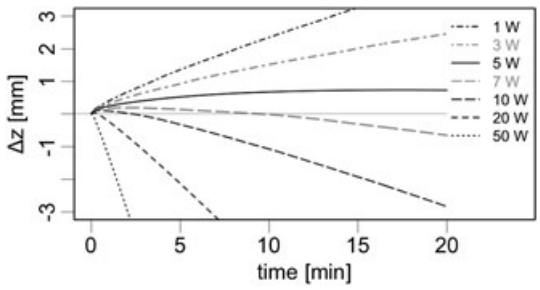


Figure 8 Modelled ice-level change ($\Delta z$) for various $P_{adv}$ with $d_{cl} = 8$ mm and $T_{rock} = -3°C$. The ice-level change becomes linear (constant erosion rate) after a stabilisation time that is shorter for a large $P_{adv}$. Symbols are given in the List of Terms.

(10 W > $P_{adv}$ > 5 W for 8-mm cleft), ice aggraded during the first seconds or minutes and was subsequently eroded or remained at a constant level if the heat flow for rock warming ($\Delta T$) balanced $P_{adv}$ (Figure 8). The time until the heat fluxes are in equilibrium and *dz/dt* becomes constant is referred to as equilibration time ($\Delta t_{eq}$).

## SYNOPSIS AND DISCUSSION

### Ice Erosion, Aggradation and Stable Conditions for Constant Heat Input

A first step towards quantitative understanding of heat advection in frozen rock clefts is to quantify $\Delta z$ and $\Delta T$ for a constant $P_{adv}$. Figure 9 shows the modelled equilibrium ice erosion rates (*dz/dt*) that result from heat input ($P_{adv}$) to a rock cleft at a given bulk temperature ($T_{rock}$). Equilibrium is reached after $\Delta t_{eq}$ = 200–4000 s. Ice erosion increases nearly linearly with heat applied for rock temperatures ranging from 0 to −5°C. The relative difference of *dz/dt* between different rock temperatures decreases with $P_{adv}$ (Figure 9). This suggests that cleft ice is eroded independently of the temperature of the surroundings for large $P_{adv}$ once the erosion equilibrium is reached (after $\Delta t_{eq}$). The decreasing influence of $T_{rock}$ is caused by the larger ratio $P_{lat}/P_{adv}$, which results from smaller thermal gradients between water and the warmed cleft surface at the water-rock interface while the ice surface remains at 0°C. The erosion rates are of the same order of magnitude as those for the stationary laboratory experiments (Figure 5). In cases where the cleft orientation deviates strongly from the modelled vertical case, less heat is consumed by ice melt (smaller $P_{lat}/P_{adv}$) due to a larger contact area of the flow cross-section and the cleft surface, and possibly because of ice remaining at the upper cleft surface.

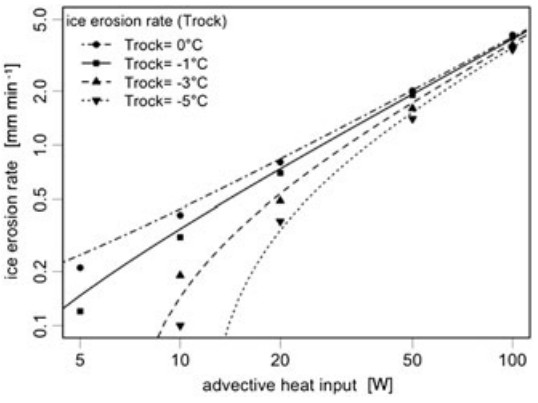


Figure 9 Modelled ice erosion rates (*dz/dt*) in relation to advective heat input ($P_{adv}$) for different rock temperatures in an 8-mm wide cleft. The points are the results from the numerical model, while the lines indicate the approximation by linear function (Equation 5). The relative difference in erosion rate decreases with larger advective heat input. This corresponds with more heat used for ice melt in relation to the applied heat ($P_{lat}/P_{adv}$). The residuals between linear approximation and model results appear larger for small erosion rates due to the logarithmic representation. Symbols are given in the List of Terms.

A multiple linear regression analysis was used to describe the ice erosion rate $dz/dt(P_{adv},T_{rock})$ after $\Delta t_{eq}$ for an 8-mm near-vertical ice-filled cleft of 0.5-m length

$$\frac{dz}{dt}[mm/\,\mathrm{min}] = (0.05 + 0.04 \cdot P_{adv} + 0.1 \cdot T_{rock}) \qquad (5)$$

with numerical values of $P_{adv}$ in W and $T_{rock}$ in °C. This linear approximation is represented by lines in Figure 9 for results from the numerical model. The quality of both the approximation and the numerical model results is low for small erosion rates and heat input due to larger relative errors. Even though extrapolation with Equation 5 to stable ice-level conditions (6.25 W) coincides with erosion rates of small $P_{adv}$ values in Figure 8, much time is needed for these rates to reach equilibrium. The laboratory experiment with small advective heat input and cold rock temperatures indicates a similar range (Equation 5 with −5°C, 11.3 W; Figure 5b, interpolation from squares ≈ 10 W). Even though Equation 5 is based on only a few results from the numerical model, it describes the dependency of the two main parameters $P_{adv}$ and $T_{rock}$. A Pearson's correlation coefficient of 0.94 was obtained when it was applied to all laboratory experiments (all cleft sizes). Equation 5 can therefore be used to provide a rough estimate of ice erosion for clefts approximately 1 cm wide, and to eliminate the length of the considered cleft, heat input per length unit (W m$^{-1}$) can be calculated by replacing the coefficient of 0.04 by 0.02 (multiplying by 0.5 m). In the Supplemental supporting material, the effect of variable heat input is discussed and can be summarised that a variable heat input causes slightly more ice erosion than a constant one and that this variability is more important if heat input is small (close to stability conditions).

### Dependency of the Erosion Rate on Timing of Advection and Conduction

Advective heat input into a cleft is usually accompanied by conductive heat from the surface. Depending on the geometric situation and the surface condition (bare rock vs snow cover), this conductive warming has differing impacts on rock temperatures around the ice level. The cyclic laboratory experiments indicate that erosion of cleft ice during a thawing event depends on the sum of applied advective heat but is also sensitive to changes in the time lag ($\Delta t$) between the start of surface warming and the start of heat advection (Figure 6b). As the data quality of these experiments is limited, these results were analysed using Equation 5. The small applied heat flux ($P_{adv}$ = 14 W) resulted in a rock temperature of −5.7°C for stability. The rock temperatures around the cleft ice level before percolation (Figure 6a) were in the range of −2° to −5°C and erosion occurred after initial aggradation. The time until the aggraded ice was completely eroded is in the order of 3 to 30 min and is very sensitive to changes in $P_{adv}$ and $T_{rock}$. If the duration of the applied flux was short, net aggradation instead of net erosion took place (see Figure 6b, cycles 8–12, 13–20 and 33–38).

The amount of heat conducted through the rock that reaches the cleft ice level after a given time depends on the latter's depth. If the ice were to aggrade over several cycles, it would reach a level where heat conduction warms the rock more rapidly and aggradation would decrease or cease. Erosion does the opposite, moving the thawing front in the cleft to colder levels and resulting in a reduced rate of erosion. That leads to stabilisation of the ice level after repeated similar cycles, as was observed in the laboratory for cycles 8–12 (while a decrease in erosion per cycle occurred for cycles 39–42, as shown in the Supplemental supporting material). In the field, this means that the ice level represents a hydrothermal equilibrium if conditions are similar on an interannual basis and if the ice level is at a depth of a few metres where annual cycles are present and temperatures decrease with depth when sensible heat advection occurs. If the cleft ice erodes to a level where thermal gradients become reversed, similar hydrothermal conditions would lead to progressive thawing over the years until lateral heat loss of the percolating water (Figure 2) is large enough to reduce heat input at the cleft ice level. This indicates that relatively small climatic variations resulting in changed inputs of water could significantly alter cleft ice conditions.

### Scaling of Conductive and Advective Heat Transport

The cleft size ($d_{cl}$) influences advective heat exchange by modifying the flow cross-section for a given discharge (changed *sf* in the model), and the ice erosion rate changes because the latent heat used for erosion depends on $d_{cl}$ (ice volume). In the laboratory, a constant $P_{adv}$ causes less ice erosion and less sensible warming if $d_{cl}$ is increased because more ice volume needs to be eroded for a given $\Delta z$ (Figure 5b).

If the whole experiment is scaled by a factor $f$ and $Q$ is multiplied by $f^2$ (proportional to the surface supplying the cleft with water of temperature $T_{win}$), the ice erosion rate remains in the same order of magnitude. For a modelled cleft with $d_{cl} = 80$ mm, for example, the erosion rate ($dz/dt$) increased by only 50 per cent compared to one with $d_{cl} = 8$ mm. This change is caused by an increase in $P_{lat}/P_{adv}$ at larger dimensions. If heat input in the up-scaled experiment lasts for factor $f$ longer (lasts longer for factor $f$), the ice-level change relative to the experiment scale remains in the same order of magnitude (e.g. increased by the 50% from the above example). For the situation including conductive heat flux (cyclic experiments), the time scaling of the two processes is not similar: in an up-scaled situation, the conductive heat wave needs $f^2$ more time to propagate from the surface to a depth increased by factor $f$ (cf. model result in Figure 3c). This different time scaling of the advective and conductive regimes ($f$ vs $f^2$, respectively) does not allow direct scaling of the cyclic experiments to annual cycles of a larger volume. The cyclic laboratory experiments, therefore, illustrate the processes but do not provide a quantitative basis for up-scaled conditions. In contrast, the stationary experiments can be transferred to other scales and allow estimates of ice erosion and rock warming in larger clefts.

## CONCLUSIONS

Several specific conclusions can be reached from this study:

1. Advective heat transport by percolating water is a highly efficient process to transmit heat from the surface to the level where clefts become impermeable. The conceptual model suggests that heat exchange with the surrounding rock takes place mainly in the area of the cleft ice level as water accumulates there and runs off laterally. Progressive thaw of cleft ice conceals the effect of warming events by export of latent heat, making them not directly detectable in ground temperature records. As a consequence, local degradation of permafrost along rock clefts may be at least partially hidden from thermal monitoring.
2. More than half of the advected sensible heat is consumed by a phase change in cleft ice erosion while the lesser portion results in rock warming. The findings from the laboratory experiments and the numerical models indicate that ice erosion occurs even in cold rock if the applied heat along a cleft is large enough ($> 28$ W m$^{-1}$ for $-6$°C and 12 W m$^{-1}$ for $-3$°C in an 8-mm cleft). This ice erosion occurs only after the cold rock has locally warmed due to latent heat released by ice aggradation during initial percolation. For large advective heat input, rock temperature has only a minor effect on the erosion rate. Conversely, percolation with only a small heat input into a cold rock cleft results in ice aggradation.
3. The main parameters that govern ice erosion and rock warming in a frozen cleft are the advective sensible heat input (resulting from water flow rate and water temperature) and rock temperature. Other factors, such as scale effects, water temperature alone (for the same heat input) and variability of flow, slightly alter the ratio between the energy used for ice erosion and rock warming but do not strongly modify the absolute values. Laboratory experiments simulating meltwater input during a thawing event indicate that the timing of the initiation of sensible heat advection relative to conductive warming from the surface is important. Given the small heat fluxes applied during these experiments, this effect is attributed to ice aggradation during initial water percolation.

A general conclusion is that rockfall, if related to warming and ice erosion in clefts, is not necessarily limited to areas with relatively warm permafrost. This may account for the low correlation observed between modelled permafrost temperature and rockfall occurrence. Furthermore, the study shows that heat applied from the surface by advection may reach failure planes at depth more rapidly and cause events of a greater magnitude than would be expected based on the assumption of conductive heat transfer.

Studies with hydrothermal models, as well as geophysics, in steep bedrock may contribute to a better understanding of permafrost degradation relating to ground ice loss. Of particular interest would be the coupling of such models with meteorological data so that the sensitivity of clefts to different meteorological situations could be assessed and compared to observed rockfall activity.

## LIST OF TERMS

| | |
|---|---|
| $\alpha$ | Inclination of the ice surface along the cleft (°) |
| $\Delta LWC$ | Change in liquid porewater content (%) |
| $\Delta t$ | Time delay between start of warming and applied advection in cyclic experiments (h) |
| $\Delta t_{eq}$ | Equilibration time needed until the ice erosion rate remains constant (s) |
| $\Delta T$ | Temperature change of rock (and ice) in the considered volume (°C) |
| $\Delta qi$ | heat flux discontinuity at the melt-interface resulting from the upward and downward heat flux *(qi_up - qi_down)* [W $m^{-2}$] |
| $\Delta z$ | Cleft ice-level change (mm) |
| $C_w$ | Heat capacity of water (volumetric liquid water): 4.18 MJ $m^{-3}$ $K^{-1}$ |
| $d_{cl}$ | Cleft width (aperture) (mm) |
| $dz/dt$ | Ice erosion rate (positive values for $\Delta z < 0$) (mm $min^{-1}$) |
| $h_{int}$ | Heat transfer coefficient for water–ice interface (W $m^{-2}$ $K^{-1}$) |
| $h_{side}$ | heat transfer coefficient for water–rock interface (sideward) in the cleft (W $m^{-2}$ $K^{-1}$) |
| $Lf$ | Latent heat of fusion (volumetric liquid water): 334 MJ $m^{-3}$ |
| $l$ | Length of cleft in experiment: constant 0.5 m |
| $P_{cond}$ | Conductive heat flux (W) |
| $P_{adv}$ | Advective heat flux (W) |
| $P_{lat}$ | Latent heat flux due to cleft ice change ($\Delta z$) (W) |
| $Q$ | Water flow (flow rate) (L $h^{-1}$) |
| $q$ | Heat flux (W $m^{-2}$) |
| $sf$ | Scaling factor for the sideways heat transfer coefficient (water–rock) ($sf = h_{side} / h_{int}$) |
| $t$ | time (experiment duration) (s) |
| $T_w$ | Mean water temperature in the cleft (empirically: $(T_{win} + T_{wout})/2$) (°C) |
| $T_{win}$ | Water temperature at the inlet (°C) |
| $T_{wout}$ | Water temperature at the outlet ( C) |
| $T_{rock}$ | Initial or undisturbed rock (and ice) temperature (°C) |
| $T_r$, $T_{r\_x}$ | Measured rock temperature within the physical model (laboratory) (°C) |
| $T_{up}$ | Temperature of upper boundary (surface in laboratory) (°C) |
| $T_{bot}$ | Temperature of lower boundary (bottom) (°C) |
| $V_w$ | Applied water volume in the cyclic experiments (L) |
| $z1$-$z5$ | Cleft ice level along the cleft at 50–450 mm from the inlet (mm) |
| $z$ | Ice level (in general, modelled, averaged) |

## ACKNOWLEDGEMENTS

The research was funded by the Swiss Federal Office for the Environment via the project PermaSense and the SNF NCCR-MICS. We would like to thank Jean-Louis Lagarde, Hansueli Gubler, Jean-Claude Ozouf and Wilfried Haeberli for their advice, many interesting discussions and sharing their long experience in geomorphodynamics, environmental physics and (lab) instrumentation. We also thank the team of the morphodynamic laboratory CNRS-M2C in Caen, France who provided a friendly welcome and supported one of us (AH) during the experiments, and M. Fabrice Freret and M. Bernard Legentil, Carrières de Montjoie, Vire, France for their availability, advice and accurate cutting of the granite blocks used for the laboratory experiment.

## REFERENCES

Boike J, Roth K, Overduin PP. 1998. Thermal and hydrologic dynamics of the active layer at a continuous permafrost site (Taymyr Peninsula, Siberia). *Water Resources Research* **34**(3): 355–363.

Boike J, Hagedorn B, Roth K. 2008. Heat and water transfer processes in permafrost-affected soils: A review of field-and modeling-based studies for the Arctic and Antarctic. In *Proceeding of the Ninth International Conference on Permafrost*, Douglas L. Kane, Kenneth M. Hinkel (eds). Institute of Northern Engineering University: Alaska Fairbanks, USA; (1): 149–154.

Dietrich P. 2005. *Flow and Transport in Fractured Porous Media*. Springer: Berlin Heidelberg, Germany.

Epstein M, Cheung FB. 1983. Complex freezing-melting interfaces in fluid flow. *Annual Review of Fluid Mechanics* **15**: 293–319.

Fischer L. 2010. Slope instabilities on perennially frozen and glacierised rock walls: multi-scale observations, analyses and modelling. PhD thesis, University of Zurich, Switzerland.

Geertsema M, Clague JJ, Schwab JW, Evans SG. 2006. An overview of recent large catastrophic landslides in northern British Columbia, Canada. *Engineering Geology* **83**(1–3): 120–143.

Gilpin RP, Hirata T, Cheng KC. 1980. Wave formation and heat transfer at an ice-water interface in the presence of a turbulent flow. *Journal of Fluid Mechanics* **99**(3): 619–640.

Gruber S, Haeberli W. 2007. Permafrost in steep bedrock slopes and its temperature-related destabilization following climate change. *Journal of Geophysical Research* **112**: F02S18.

Gruber S, Hoelzle M, Haeberli W. 2004. Permafrost thaw and destabilization of Alpine rock walls in the hot summer of 2003. *Geophysical Research Letters* **31**(13): L13504.

Haeberli W, Beniston M. 1998. Climate change and Its impacts on glaciers and permafrost in the Alps. *Ambio* **27**(4): 258–265.

Haeberli W, Wegmann M, Vonder Muehll D. 1997. Slope stability problems related to glacier shrinkage and permafrost degradation in the Alps. *Ecologae Geologicae Helvetiae* **90**(3): 407–414.

Harris C, Davies MCR, Etzelmueller B. 2001. The assessment of potential geotechnical hazards associated with mountain permafrost in a warming global climate. *Permafrost and Periglacial Processes* **12**(1): 145–156. DOI: 10.1002/ppp.376.

Harris C, Kern-Luetschg M, Murton J, Font M, Davies M, Smith F. 2008. Solifluction processes on permafrost and non-permafrost slopes: results of a large-scale laboratory simulation. *Permafrost and Periglacial Processes* **19**(4): 359–378. DOI: 0.1002/ppp.630.

Harris C, Arenson LU, Christiansen HH, Etzelmüller B, Frauenfelder R, Gruber S, Haeberli W, Hauck C, Hölzle M, Humlum O. 2009. Permafrost and climate in Europe: Monitoring and modelling thermal, geomorphological and geotechnical responses. *Earth-Science Reviews* **92**(3–4): 117–171.

Hasler A. 2011. Thermal conditions and kinematics of steep bedrock permafrost. PhD thesis, University of Zurich, Switzerland.

Hasler A, Gruber S, Haeberli W. 2011. Temperature variability and thermal offset in steep alpine rock and ice faces. *The Cryosphere Discussion* **5**: 721–753.

Kane DL, Hinkel KM, Goering DJ, Hinzman LD, Outcalt SI. 2001. Non-conductive heat transfer associated with frozen soils. *Global and Planetary Change* **29**(3–4): 275–292.

Krautblatter M, Hauck C. 2007. Electrical resistivity tomography monitoring of permafrost in solid rock walls. *Journal of Geophysical Research* **112**: F02S20.

Noetzli J, Hoelzle M, Haeberli W. 2003. Mountain permafrost and recent Alpine rock-fall events: A GIS-based approach to determine critical factors. In *Proceedings of Eighth International Conference on Permafrost*, Phillips M, Springman SM, Arenson LU. (eds). Swets & Zeitlinger: Lisse, Netherlands(1): 827–832.

Pogrebiskiy MI, Chernyshev SN. 1977. Determination of the Permeability of the Frozen Fissured Rock Massif in the Vicinity of the Kolyma Hydroelectric Power Station (Oshenka Vodopronishaemosti Merzlogo Greshinovatogo Massiva Gornkh Porod Uchastka Kolmskoy ges). Cold Regions Research and Engineering Laboratory, Hanover, NH.

Rist A. 2007. Hydrothermal processes within the active layer above alpine permafrost in steep scree slopes and their influence on slope stability. PhD thesis, University of Zürich, Switzerland.

Rist A, Phillips M. 2005. First results of investigations on hydrothermal processes within the active layer above alpine permafrost in steep terrain. *Norwegian Journal of Geography* **59**(2): 177–183.

Scherler M, Hauck C, Hoelzle M, Stähli M, Völksch I. 2010. Meltwater infiltration into the frozen active layer at an alpine permafrost site. *Permafrost and Periglacial Processes* **21**(4): 325–334. DOI: 10.1002/ppp.694.

Stähli M, Jansson P, Lundin L. 1996. Preferential water flow in a frozen soil - a two-domein model approach. *Hydrological Processes* **10**(10): 1305–1316.